International Journal of Bifurcation and Chaos, Vol. 22, No. 10 (2012) 1250246 (14 pages)

DOI: 10.1142/S021812741250246X

COMPLEX DYNAMICS OF SEMICONDUCTOR QUANTUM DOT LASERS SUBJECT TO DELAYED OPTICAL FEEDBACK

CHRISTIAN OTTO*, BJÖRN GLOBISCH, KATHY LÜDGE
and ECKEHARD SCHÖLL
Institut für Theoretische Physik, Technische Universität Berlin,
Hardenbergstraße 36, 10623 Berlin, Germany
**christian.otto@tu-berlin.de*

THOMAS ERNEUX
Université Libre de Bruxelles, Optique Nonlinéaire Théorique,
Campus Plaine, C.P. 231, 1050 Bruxelles, Belgium
terneux@ulb.ac.be

Received March 28, 2011; Revised August 10, 2011

We study a five-variable electron-hole model for a quantum-dot (QD) laser subject to optical feedback. The model includes microscopically computed Coulomb scattering rates. We consider the case of a low linewidth enhancement factor and a short external cavity. We determine the bifurcation diagram of the first three external cavity modes and analyze their bifurcations. The first Hopf bifurcation marks the critical feedback rate below which the laser is stable. We derive an analytical approximation for this critical feedback rate that is proportional to the damping rate of the relaxation oscillations (ROs) and inversely proportional to the linewidth enhancement factor. The damping rate is described in terms of the carrier lifetimes. They depend on the specific band structure of the QD device and they are computed numerically.

Keywords: Quantum-dot laser; optical feedback; Lang–Kobayashi model.

1. Introduction

The exceptional performance of self-assembled quantum-dot materials renders them extremely appealing for their use as optical communications devices. As lasers, they feature reduced and temperature independent threshold current and proper emission wavelength at the fiber telecommunication windows. These properties, together with the low linewidth enhancement factor and broad spectrum, make QD materials extremely attractive for application as light emitters or amplifiers.

There exist, nevertheless, several unclear issues which prevent QDs from leading the new generation of optoelectronic devices. Their differential efficiency is lower than expected. The output power of QD lasers is lower than that of their Quantum Well (QW) counterpart. Still, it is their dynamical stability properties which have initiated most of the studies. In particular, their higher tolerance to optical feedback compared to QW semiconductor lasers is important for data transmission in fiber optic telecom applications. Intensive theoretical and experimental work has been carried out in order to understand which laser parameters (or group of parameters) may have an impact on the stability of the laser. For the QW laser, a sufficient condition for stability has been derived in terms of a critical feedback rate k_c below which the laser is guaranteed to

be stable. This condition has the form [Mørk *et al.*, 1992]

$$k < k_c := \frac{\Gamma_R}{\sqrt{1+\alpha^2}} \tag{1}$$

where Γ_R represents the damping rate of the Relaxation Oscillations (ROs) and α is the linewidth enhancement factor. Although derived from the standard QW laser rate equations, Eq. (1) is used as a guide in current experimental studies of QD lasers [Azouigui *et al.*, 2009; Grillot *et al.*, 2008; O'Brien *et al.*, 2003; Gioannini *et al.*, 2008]. A laser with a strong RO damping rate and with a low α will be less sensitive to optical feedback. For the QW laser, this can be realized by increasing the lifetime of the photons in the cold cavity to a value comparable to the carrier lifetime while maintaining strict single mode operation [Baili *et al.*, 2006, 2009]. For the QD laser, the task is much more subtle because carrier lifetimes and α strongly depend on material design as well as operating conditions (wavelength and pump parameter). A linewidth enhancement factor as small as 0.1 was reported for injection current below threshold [Newell *et al.*, 1999], however, it increases above threshold reaching values close to those of QW lasers [Cong *et al.*, 2007; Ramdane *et al.*, 2008]. Current publications report on QD lasers that exhibit either a large or a low value of α [Grillot & Dubey, 2011; Lin *et al.*, 2011].

We consider a five-variable electron-hole model for a QD laser. Our model combines Lang–Kobayashi (LK) type field equations [Lang & Kobayashi, 1980] with microscopically based rate equations for the carriers that have also been incorporated in models for semiconductor optical amplifiers [Majer *et al.*, 2010; Wegert *et al.*, 2011]. The solitary laser has been studied previously in [Lüdge & Schöll, 2009; Lüdge *et al.*, 2010, 2011] and the dynamics of the model subject to optical feedback has been studied in [Otto *et al.*, 2010]. In this paper, we analyze the simplest case of a laser exhibiting a low linewidth enhancement factor and subject to optical feedback from a mirror close to the laser (short external cavity). We determine numerically the bifurcation diagram of the first three external cavity modes (ECMs) and investigate systematically each of their bifurcations. As we shall demonstrate, the bifurcation diagram exhibits complex dynamics even with a single ECM. We then concentrate on the first Hopf bifurcation point that marks the critical feedback rate below which the laser is stable. We determine a simple analytical approximation of the form (1) but now with a new expression for Γ_R. The numerical validity of this approximation is tested using a numerical continuation method. We conclude that it is the relatively larger value of Γ_R that explains the higher stability properties of QD lasers.

The paper is organized as follows. We introduce the laser rate equations in Sec. 2 and determine the ECMs in Sec. 3. Section 4 describes a typical numerical bifurcation diagram which involves the first three ECMs. We determine an approximation of the first Hopf bifurcation point in Sec. 5 and summarize our main results in Sec. 6.

2. Laser Model

In this section, the electron-hole rate equation model for a QD laser with optical feedback from a distant mirror is introduced. A schematic setup of the device is depicted in Fig. 1. In the QD laser model carriers are first injected into a two-dimensional carrier reservoir before they are captured by the QDs. The nonlinear rate equations describe the dynamics of the photon density $n_{\rm ph}$ and the phase ϕ of the complex, slowly varying electrical field amplitude $\mathcal{E}(t) := \sqrt{An_{\rm ph}(t)}e^{-i\phi(t)}$ where A is the active area as well as the dynamics of the carriers. Photon density and phase variables, labeled by the subscript $\tau_{\rm ec}$ denote quantities taken at time points $t-\tau_{\rm ec}$ that are delayed by the round-trip time of the light in the external cavity $\tau_{\rm ec}$ (for example: $n_{{\rm ph},\tau_{\rm ec}} := n_{\rm ph}(t-\tau_{\rm ec})$). For the carriers separate rate equations are formulated for electron and hole densities in the quantum dots, n_e and n_h, as well as for electron- and hole densities in the carrier

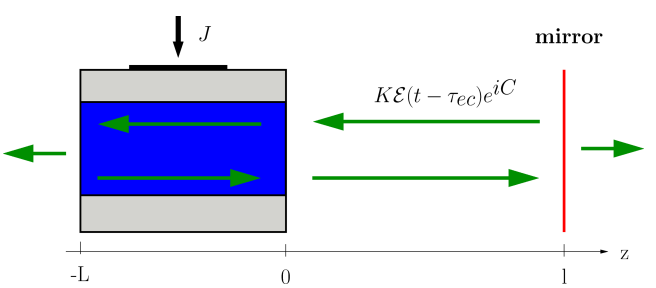

Fig. 1. Schematic setup of the considered laser device with delayed optical feedback from an external cavity. The electrical field amplitude $\mathcal{E}$ taken at a time $t-\tau_{\rm ec}$ delayed by the external cavity round trip time $\tau_{\rm ec}$ is coupled back into the laser multiplied with the feedback strength K and rotated by the external cavity phase C.

reservoir, denoted by w_e and w_h, respectively. The complete system of delay differential equations reads:

$$\dot{n}_{\rm ph} = -2\kappa n_{\rm ph} + \Gamma R_{\rm ind}(n_e, n_h, n_{\rm ph}) + \beta R_{\rm sp}(n_e, n_h) + 2\frac{K}{\tau_{\rm in}}\sqrt{n_{{\rm ph},\tau_{\rm ec}} n_{\rm ph}}\cos(\phi - \phi_{\tau_{\rm ec}} + C), \tag{2}$$

$$\dot{\phi} = \frac{\alpha}{2}[\Gamma WA(n_e + n_h - N^{\rm QD}) - 2\kappa] - \frac{K}{\tau_{\rm in}}\sqrt{\frac{n_{{\rm ph},\tau_{\rm ec}}}{n_{\rm ph}}}\sin(\phi - \phi_{\tau_{\rm ec}} + C), \tag{3}$$

$$\dot{n}_e = S_e^{\rm in}(w_e, w_h)(N^{\rm QD} - n_e) - S_e^{\rm out}(w_e, w_h)n_e - R_{\rm ind}(n_e, n_h, n_{\rm ph}) - R_{\rm sp}(n_e, n_h), \tag{4}$$

$$\dot{n}_h = S_h^{\rm in}(w_e, w_h)(N^{\rm QD} - n_h) - S_h^{\rm out}(w_e, w_h)n_h - R_{\rm ind}(n_e, n_h, n_{\rm ph}) - R_{\rm sp}(n_e, n_h), \tag{5}$$

$$\dot{w}_e = \frac{j}{e_0} + \frac{N^{\rm sum}}{N^{\rm QD}}(S_e^{\rm in}(w_e, w_h) + S_e^{\rm out}(w_e, w_h))n_e - S_e^{\rm in}(w_e, w_h)N^{\rm sum} - \tilde{R}_{\rm sp}(w_e, w_h), \tag{6}$$

$$\dot{w}_h = \frac{j}{e_0} + \frac{N^{\rm sum}}{N^{\rm QD}}(S_h^{\rm in}(w_e, w_h) + S_h^{\rm out}(w_e, w_h))n_h - S_h^{\rm in}(w_e, w_h)N^{\rm sum} - \tilde{R}_{\rm sp}(w_e, w_h). \tag{7}$$

In the photon equation [Eq. (2)] the optical intensity loss 2κ is balanced by the linear gain term $\Gamma R_{\rm ind}$. Therein Γ is the optical confinement factor and the linear gain, resulting from the inversion in the quantum dots, is given by $R_{\rm ind}(n_e, n_h, n_{\rm ph}) := WA(n_e + n_h - N^{\rm QD})n_{\rm ph}$, with the Einstein-factor W, the normalization area of the QDs A, and twice the density of the subensemble of active quantum dots $N^{\rm QD}$ (the factor of two accounts for spin degeneracy). The spontaneous emission in the QDs and in the carrier reservoir is modeled by bimolecular recombinations $R_{\rm sp}(n_e, n_h) := (W/N^{QD})n_e n_h$ and $\tilde{R}_{\rm sp}(w_e, w_h) := B^S w_e w_h$, respectively, with the band–band recombination coefficient in the carrier-reservoir B^S. In the equation for the optical subsystem [Eq. (2)] the expression $R_{\rm sp}$ for the spontaneous emission is multiplied with the spontaneous emission factor β, which takes into account that only a small fraction of the photons generated by spontaneous emission have the same wavelength as the lasing mode. The linewidth enhancement factor that models the phase-amplitude coupling is denoted by α. We are aware of the fact that for QD lasers this quantity α is problematic because it cannot account for the independent dynamics of resonant (n_e, n_h) and nonresonant (w_e, w_h) charge carriers and eventually neglects a degree of freedom of the dynamics. For a careful treatment of this topic, see [Lingnau *et al.*, 2012] and [Gioannini *et al.*, 2006]. However, in this paper we want to focus on an analytical treatment and choose a constant α for sake of simplicity. The last term in Eqs. (2) and (3), respectively, models the effect of the optical feedback. The feedback strength K varies from zero to one, the internal cavity round-trip time is denoted by $\tau_{\rm in}$ and C is the phase with which the light is coupled back into the cavity. It is given by $C := \omega_{\rm th}\tau_{\rm ec}$, with the frequency $\omega_{\rm th}$ of the solitary laser at lasing threshold. Variations of the phase over its full range $[0, 2\pi]$ can be obtained by very small variations of the length of the external cavity by half of the optical wavelength ($\lambda/2 \sim 650\,{\rm nm}$). Since this variation does not significantly modify the external cavity round-trip time $\tau_{\rm ec}$ itself, C is regarded as an independent parameter. The carriers are first injected into the carrier reservoir with the current density j, and e_0 is the elementary charge. Carrier exchange between carrier reservoir and QDs is mediated by the nonlinear, microscopically calculated Coulomb scattering rates, that are denoted by $S_e^{\rm in}$ and $S_h^{\rm in}$ for electron and hole capture into the QD levels and by $S_e^{\rm out}$ and $S_h^{\rm out}$ for carrier escape to the reservoir, respectively. The scattering rates depend upon the reservoir densities and determine the carrier lifetime for electrons $\tau_e := (S_e^{\rm in} + S_e^{\rm out})^{-1}$ and holes $\tau_h := (S_h^{\rm in} + S_h^{\rm out})^{-1}$, respectively. Twice the total quantum dot density is denoted by $N^{\rm sum}$, thus $N^{\rm QD}/N^{\rm sum}$ is the fraction of QDs that participate at the emission of the laser light.

To simplify notation we wish to discuss the rate equations in a dimensionless form, that has already been introduced in [Lüdge *et al.*, 2011] for the solitary laser. If not stated otherwise, we use the same values of the original physical parameters as in [Otto *et al.*, 2010]. Please note that in [Globisch *et al.*, 2012] and [Pausch *et al.*, 2012] a different terminology is used. The differences to the notation of this paper are explained in the appendices of these publications. To reformulate the

equations in dimensionless form, we introduce the new dimensionless variables $N_{\rm ph}$, $N_{e/h}$, $W_{e/h}$ and t' defined by:

$$\begin{aligned} n_{\rm ph} = A^{-1}N_{\rm ph}, \quad n_{e/h} = N^{\rm QD}N_{e/h}, \\ w_{e/h} = N^{\rm sum}W_{e/h}, \quad t' := 2\kappa t. \end{aligned} \tag{8}$$

Inserting Eq. (8) into Eqs. (2)–(7), and neglecting spontaneous emission in the optical equations ($\beta = 0$), yields:

$$N'_{\rm ph} = [g(N_e + N_h - 1) - 1]N_{\rm ph} + 2k\sqrt{N_{\rm ph}N_{{\rm ph},\tau}}\cos(C - \phi_\tau + \phi), \tag{9}$$

$$\phi' = \frac{\alpha}{2}[g(N_e + N_h - 1) - 1] - k\sqrt{\frac{N_{{\rm ph},\tau}}{N_{\rm ph}}}\sin(C - \phi_\tau + \phi), \tag{10}$$

$$N'_e = \gamma[s_e^{\rm in}(W_e, W_h)(1 - N_e) - s_e^{\rm out}(W_e, W_h)N_e - (N_e + N_h - 1)N_{\rm ph} - N_eN_h], \tag{11}$$

$$N'_h = \gamma[s_h^{\rm in}(W_e, W_h)(1 - N_h) - s_h^{\rm out}(W_e, W_h)N_h - (N_e + N_h - 1)N_{\rm ph} - N_eN_h], \tag{12}$$

$$W'_e = \gamma[J + (s_e^{\rm in}(W_e, W_h) + s_e^{\rm out}(W_e, W_h))N_e - s_e^{\rm in}(W_e, W_h) - cW_eW_h], \tag{13}$$

$$W'_h = \gamma[J + (s_h^{\rm in}(W_e, W_h) + s_h^{\rm out}(W_e, W_h))N_h - s_h^{\rm in}(W_e, W_h) - cW_eW_h]. \tag{14}$$

Here prime ($'$) means differentiation with respect to the dimensionless time t'. The dimensionless out-scattering rates $s_e^{\rm out}$, $s_h^{\rm out}$ and the parameters g, k, τ, γ, J and c introduced above are defined as follows:

$$\begin{gathered} s_{e/h}^{\rm in/out} := \frac{1}{W}S_{e/h}^{\rm in/out}, \quad g := \frac{\Gamma WAN^{\rm QD}}{2\kappa}, \quad k := \frac{1}{2\kappa}\frac{K}{\tau_{\rm in}}, \quad \tau := 2\kappa\tau_{\rm ec}, \\ \gamma := \frac{W}{2\kappa}, \quad J := \frac{j}{e_0N^{\rm sum}W}, \quad c := \frac{B^SN^{\rm sum}}{W}. \end{gathered}$$

The dimensionless electron- and hole lifetimes are denoted by $t_e := (s_e^{\rm in} + s_e^{\rm out})^{-1}$ and $t_h := (s_h^{\rm in} + s_h^{\rm out})^{-1}$, respectively. The parameter values that have been used in our numerical simulations are shown in Table 1.

Table 1. Dimensionless parameters for Eqs. (9)–(14), that correspond to the physical parameters given in [Otto *et al.*, 2010].

Parameters	Value	Meaning
g	3.78	Linear gain parameter
γ	7×10^{-3}	Ratio of photon and carrier lifetime
k	$K/2.4$	Rescaled feedback strength
τ	16	External cavity round-trip time
c	1.54	Spontaneous and nonradiative losses
$J/J_{\rm th}$	2.50	Ratio of current to current at lasing threshold
$J_{\rm th}$	3.96	Current at lasing threshold
$N_{\rm ph}$	3.16	Steady state photon population at $J/J_{\rm th} = 2.5$ for $k = 0$
N_e (N_h)	0.83 (0.44)	Steady state electron (hole) population at $J/J_{\rm th} = 2.5$ for $k = 0$
W_e (W_h)	2.20 (2.59)	Steady state electron (hole) density in carrier reservoir at $J/J_{\rm th} = 2.5$ for $k = 0$
$s_e^{\rm in}$ ($s_h^{\rm in}$)	7.32 (15.40)	Steady state electron (hole) in-scattering rates at $J/J_{\rm th} = 2.5$ for $k = 0$
$s_e^{\rm out}$ ($s_h^{\rm out}$)	9.70×10^{-2} (16.94)	Steady state electron (hole) out-scattering rates at $J/J_{\rm th} = 2.5$ for $k = 0$
t_e	1.35×10^{-1}	Steady state electron lifetime at $J/J_{\rm th} = 2.5$ for $k = 0$
t_h	3.09×10^{-2}	Steady state hole lifetime at $J/J_{\rm th} = 2.5$ for $k = 0$

3. Basic Solutions — The External Cavity Modes (ECMs)

Equations (9)–(14) are not independent, but contain carrier conservation as we can see by calculating the quantity

$$N_e' - N_h' + W_e' - W_h' = 0.$$

Thus, the term $N_e - N_h + W_e - W_h$ is a constant that is determined by the initial conditions. Physically we can describe the effect of reservoir doping by choosing a nonzero initial value for one of the reservoir densities, i.e. $W_e \neq 0$ for n-doping and $W_h \neq 0$ for p-doping, respectively [Lüdge & Schöll, 2010]. In the absence of doping this constant is zero:

$$N_e - N_h + W_e - W_h = 0. \tag{15}$$

Due to the invariance of the dynamical equations (9)–(14) under rotations in the complex plane ($\mathbb{S}^1$-Symmetry), their basic solutions are rotating waves with constant photon and carrier numbers and a phase that varies linearly in time [Krauskopf *et al.*, 2000], i.e. they are special periodic orbits with circular shape:

$$\begin{aligned}(N_{\mathrm{ph}}(t'), \phi(t'), N_e(t'), N_h(t'), W_e(t'), W_h(t'))^\top \\ = \left(\sqrt{N_{\mathrm{ph},s}}, \left(-\frac{C}{\tau} + \omega_s\right) t', N_{e,s}, \right. \\ \left. N_{h,s}, W_{e,s}, W_{h,s}\right)^\top. \end{aligned} \tag{16}$$

Solutions, given by Eq. (16) are called external cavity modes (ECMs). The frequency deviation of the ECM-frequency ω from the frequency of the solitary laser at its lasing threshold is given by $\omega_s - C/\tau$. Inserting the ECM ansatz Eq. (16) into Eqs. (9) and (10), we find the following expression for nonzero intensity solutions ($N_{\mathrm{ph},s} \neq 0$):

$$\begin{aligned} N^{\mathrm{inv}} &:= \frac{1}{2}[g(N_{e,s} + N_{h,s} - 1) - 1] \\ &= -k\cos(\omega_s \tau), \end{aligned} \tag{17}$$

$$\omega_s - \frac{C}{\tau} = \alpha N^{\mathrm{inv}} - k\sin(\omega_s \tau). \tag{18}$$

In Eq. (17) a carrier inversion N^{inv} which is zero at the threshold of the solitary laser has been introduced. (See Sec. 4 for a plot of the carrier inversions N^{inv} and the frequency deviations $\omega_s - C/\tau$ in terms of the feedback strength k.) Without feedback ($k = 0$) we see from Eq. (17), that the sum of the electron and hole numbers in the quantum dots $N_e + N_h = (1 + g)/g$ is "clamped" to a constant value. This is the well-known effect of gain-clamping in semiconductor lasers [van Tartwijk & Lenstra, 1995]. With feedback ($k \neq 0$), Eq. (17) demonstrates the effect of threshold reduction. For suitable values of ω_s, the right-hand side of Eq. (17) becomes negative, which means that the carrier population necessary for inversion and thus the lasing threshold is reduced in comparison to the solitary laser.

With the help of the relation for the carrier conservation [Eq. (15)] we can express the QD populations $N_{e,s}$ and $N_{h,s}$ as functions of the reservoir populations $W_{e,s}$ and $W_{h,s}$:

$$N_{e,s} = \frac{1}{2}\left[\frac{1 + g - 2k\cos(\omega_s \tau)}{g} + W_{h,s} - W_{e,s}\right], \tag{19}$$

$$N_{h,s} = \frac{1}{2}\left[\frac{1 + g - 2k\cos(\omega_s \tau)}{g} + W_{e,s} - W_{h,s}\right]. \tag{20}$$

From Eqs. (13) and (14), we find that the reservoir populations have to be determined by solving the equations

$$\begin{aligned} J + (s_e^{\mathrm{in}}(W_{e,s}, W_{h,s}) + s_e^{\mathrm{out}}(W_{e,s}, W_{h,s}))N_{e,s} \\ - s_e^{\mathrm{in}}(W_{e,s}, W_{h,s}) - cW_{e,s}W_{h,s} = 0, \end{aligned} \tag{21}$$

$$\begin{aligned} J + (s_h^{\mathrm{in}}(W_{e,s}, W_{h,s}) + s_h^{\mathrm{out}}(W_{e,s}, W_{h,s}))N_{h,s} \\ - s_h^{\mathrm{in}}(W_{e,s}, W_{h,s}) - cW_{e,s}W_{h,s} = 0, \end{aligned} \tag{22}$$

self-consistently, which has to be done numerically due to the nonlinear functions for the scattering rates. Taking the ECM ansatz [Eq. (16)] the evolution equations for the carrier populations [Eqs. (11)–(14)] equate to zero. By inserting Eqs. (13) and (14) into Eqs. (11) and (12) we get an expression for $N_{\mathrm{ph},s}$ as a function of the carrier populations:

$$\begin{aligned} N_{\mathrm{ph},s} = \frac{g}{1 - 2k\cos(\omega_s \tau)} \\ \times [J - N_{e,s}N_{h,s} - cW_{e,s}W_{h,s}]. \end{aligned} \tag{23}$$

The carrier populations do not vary significantly above threshold. Thus, we retrieve in good approximation the linear dependence of $N_{\mathrm{ph},s}$ on the pumping current, which is typical for semiconductor

lasers above the threshold:

$$N_{\mathrm{ph},s} \propto J - J_{\mathrm{th}}, \tag{24}$$

where we have introduced the threshold current of the solitary laser $J_{\mathrm{th}} := N_{e,\mathrm{th}}N_{h,\mathrm{th}} + cW_{e,\mathrm{th}}W_{h,\mathrm{th}}$. The carrier populations $N_{e/h,\mathrm{th}}$ and $W_{e/h,\mathrm{th}}$ are defined at the threshold of the solitary laser.

In the following subsections we aim to derive expressions for the line at which new pairs of ECMs are created in saddle-node bifurcations and the ellipse on which the ECMs lie. In terms of the frequency deviation $\omega_s - C/\tau$ and the inversion N^{inv} they are identical to the expressions that have been derived for the LK model. For a more detailed discussion please consider, for example, the review article by van Tartwijk and Agrawal [1998] or the article by Rottschäfer and Krauskopf [2007].

3.1. *Line of saddle-node bifurcations*

With increasing feedback strength ECMs are formed pairwise in saddle-node bifurcations (see Sec. 4). To see this we insert Eq. (17) into Eq. (18):

$$\omega_s - \frac{C}{\tau} = -k(\alpha\cos(\omega_s\tau) + \sin(\omega_s\tau)). \tag{25}$$

With the help of some trigonometric relations, this can be rewritten as

$$\omega_s - \frac{C}{\tau} = -\frac{K_e}{\tau}\sin(\omega_s\tau + \arctan(\alpha)), \tag{26}$$

where we have introduced the effective feedback strength $K_e := k\tau\sqrt{1+\alpha^2}$. See [Rottschäfer & Krauskopf, 2007] for a nice graphical interpretation of Eq. (26). For a saddle-node bifurcation to occur, the derivatives with respect to ω_s on both sides of Eq. (26) have to be equal. This provides us with the condition

$$-\frac{1}{K_e} = \cos(\omega_s\tau + \arctan(\alpha)). \tag{27}$$

Equation (27) has solutions for $K_e \geq 1$. Thus for $K_e < 1$ the equation for the frequency deviation [Eq. (18)] has only one solution, namely the ECM that results from the solution of the solitary laser. For $K_e \geq 1$ new pairs of ECMs are created pairwise in saddle-node bifurcations. The saddle-solutions are called anti-modes and they are unstable upon their creation. The stability of the node solutions, which are called modes, has to be determined by a linear stability analysis. This is going to be discussed in Sec. 4. To get an expression for the inversion along the saddle-node lines $N^{\mathrm{inv}}_{\mathrm{sn}}$ in terms of the frequency deviation $\omega_s - C/\tau$ of the ECMs, we apply the saddle-node condition, i.e. taking the derivative of both sides of Eq. (25) with respect to ω_s and requiring equality, which yields

$$1 = \tau(\alpha k\sin(\omega_s\tau) - k\cos(\omega_s\tau)). \tag{28}$$

Inserting Eqs. (17) and (18) in the above expression provides us with the expression for the line of saddle-node bifurcation in the $(\omega_s - C/\tau, N^{\mathrm{inv}})$-plane:

$$N^{\mathrm{inv}}_{\mathrm{sn}}\left(\omega_s - \frac{C}{\tau}\right) = \frac{1 + \tau\alpha\left(\omega_s - \dfrac{C}{\tau}\right)}{\tau(1+\alpha^2)}. \tag{29}$$

Anti-modes are associated with destructive interference of the laser field and the field delayed by the external cavity round-trip time τ, and modes are associated with constructive interference [Levine *et al.*, 1995]. Anti-modes lie above the saddle-node line while modes lie below this line [Rottschäfer & Krauskopf, 2007].

3.2. *Ellipse of ECMs*

In the $(\omega_s - C/\tau, N^{\mathrm{inv}})$-plane the ECM solutions lie on an ellipse that is well known for the LK model. This can be seen by rewriting Eq. (18) as $\omega_s - C/\tau - \alpha N^{\mathrm{inv}} = -k\sin(\omega_s\tau)$, and adding the square of this equation to the square of Eq. (17):

$$\left(\omega_s - \frac{C}{\tau} - \alpha N^{\mathrm{inv}}\right)^2 + (N^{\mathrm{inv}})^2 = k^2. \tag{30}$$

In Sec. 4 the ellipse is plotted for different values of k. ECMs are created at intersection points of the ellipse [Eq. (30)] with the line of saddle-node bifurcations [Eq. (29)]. For $K_e > 1$, we find two solutions ω_{sn}:

$$\omega_{\mathrm{sn}} - \frac{C}{\tau} = \pm\frac{1}{\tau}\sqrt{K_e^2 - 1}. \tag{31}$$

4. Bifurcation Analysis

In this section we analyze the stability of the ECM solutions [Eq. (16)] of the dynamical Eqs. (9)–(14) and compare our findings with direct numerical simulations. According to experimental findings QD lasers seem to have a smaller phase-amplitude coupling than QW lasers [Newell *et al.*, 1999]. Thus we focus on the case of small $\alpha = 0.9$. Further, having in mind integrated devices, we focus on the short-cavity regime as introduced by Schunk and

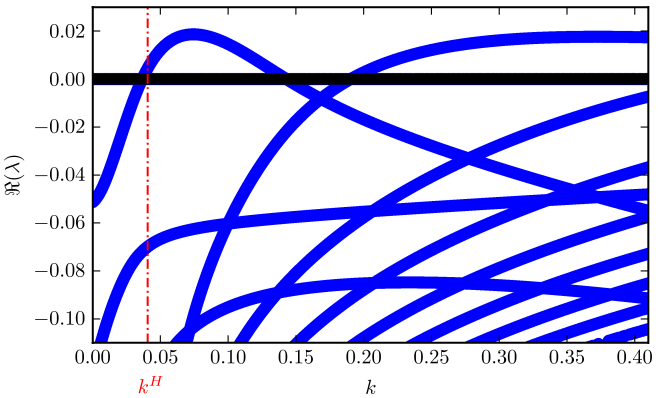

Fig. 2. Real parts of the Floquet exponent (solid blue lines) of the ECM that can be followed out of the solitary laser solution in terms of the feedback-strength k. The horizontal (black) line corresponds to the trivial Floquet-multiplier (Goldstone mode). The vertical red dash-dotted line indicates the feedback strength k^H at which the first supercritical Hopf bifurcation occurs. Parameters: $\alpha = 0.9$, $\tau = 16$, $C = \pi$, other parameters as in Table 1.

Petermann [1989]. The authors define an external cavity as short if the product of the RO frequency and the roundtrip time of the light in the external cavity is considerably less than unity. Since Eqs. (9) and (10) are delay differential equations, each mode has infinitely many eigenvalues. Their real parts rise from minus infinity with increasing feedback strength. In Fig. 2 the real parts of the eigenvalues of the first ECM (the one that can be followed out of the solution for the solitary laser) are plotted over the feedback strength k. The transcendential characteristic equation has been solved numerically. At a critical feedback strength $k^H = 0.041$ (red dash-dotted lines in Figs. 2 and 3) the leading eigenvalue crosses the real axis and the mode becomes unstable in a supercritical Hopf bifurcation leading to a more complex solution with periodically modulated photon population. In the following, we are going to study the dynamics of the laser in

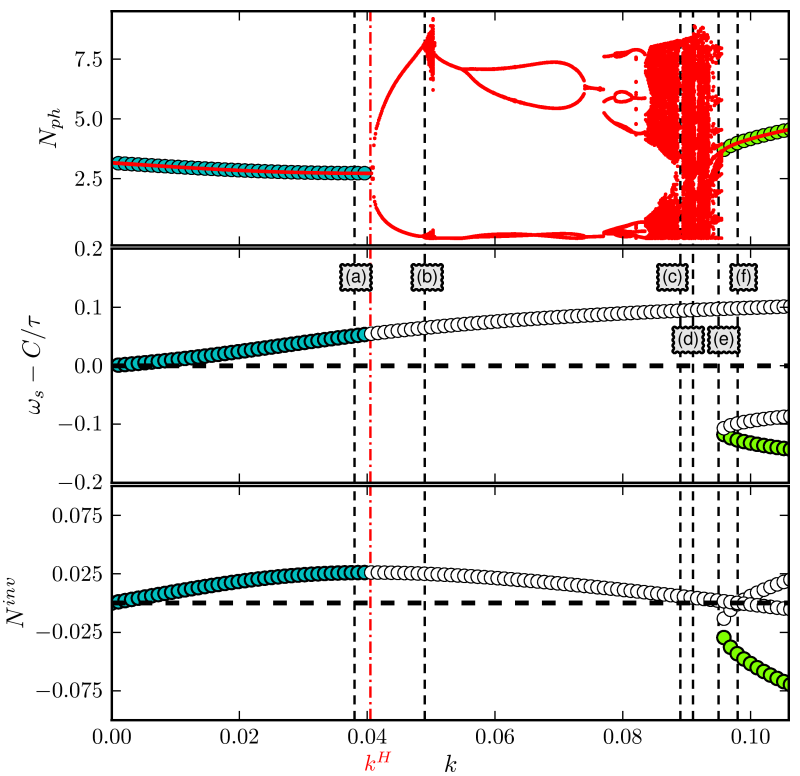

Fig. 3. (Upper panel) Bifurcation diagram of the photon number N_{ph} (red points) as a function of the rescaled feedback strength k. Filled circles are steady state values of N_{ph} of the stable ECMs. (Middle and lower panel) Frequency deviations $\omega_s - C/\tau$ and carrier inversion N^{inv} of the ECMs as functions of k. Filled circles indicate stability of the ECM and open circles indicate its instability. Vertical black dashed lines labeled (a) to (f) mark k-values at which time series and phase space projections are shown in Figs. 4 and 5, respectively. The feedback strength of the first supercritical Hopf bifurcation is labeled k^H (vertical red dash-dotted line). Parameters: $\alpha = 0.9$, $\tau = 16$, $C = \pi$, other parameters as in Table 1.

the unstable regime. In the short cavity regime for $\tau = 16$ and for small $\alpha = 0.9$ the laser displays only one instability region as a function of the feedback strength k.

In the following we are going to focus on this region of the bifurcation diagram. In the upper panel of Fig. 3, the bifurcation diagram of $N_{\rm ph}$ as a function of k is plotted with red dots. Here we plot the local extrema of $N_{\rm ph}$ for each value of k after transients have died out. Additionally the photon population $N_{{\rm ph},s}$ of the first and the second ECM given by Eq. (23) are plotted in the upper panel of Fig. 3. Stable ECMs are indicated by filled circles. The middle panel shows the frequency deviations $\omega_s - C/\tau$ of the ECMs and in the lower panel the carrier inversion $N^{\rm inv}$ of the ECMs is plotted as a function of k. Stable modes are indicated by filled and unstable modes by open circles. Vertical black dashed lines labeled by (a) to (f) indicate k-values at which time series and phase space projections are presented in Figs. 4 and 5, respectively. In Fig. 5 the trajectory (red solid line) is projected onto a plane spanned by the frequency deviations and the carrier inversion. In this projection, ECMs are points. For more complex solutions with nonconstant frequency ω_s, we plot the frequency deviations averaged over one external cavity round-trip time τ. They are given by $(\phi - \phi_\tau)/\tau$. The ECMs lie on the ellipse described by Eq. (30) (black dashed line in Fig. 5). On the blue dash-dotted line in Fig. 5 saddle-node bifurcations take place [Eq. (29)]. Note that the saddle-node line and the ellipse of the ECM are plotted as functions of the frequency deviation $\omega_s - C/\tau$, while the ECMs and the trajectories of more complex solutions are only plotted for the fixed value $C = \pi$ of the phase. For $C = \pi$ the saddle-node bifurcation takes place at a feedback strength $k = 0.08955$ (see Fig. 3, middle and lower panel). Also in Fig. 5 stable ECMs are indicated by filled circles. The filling color corresponds to the color-code of the stable modes in Figs. 3 and 4. Unstable ECMs, modes as well as anti-modes, are indicated by gray open circles.

At $k = 0$ the first ECM is stable. With increasing k its frequency and its carrier inversion shift. This is why in Fig. 5(a) the ECM is not located at the origin (see also black dashed line labeled (a) in Fig. 3). At $k^H = 0.0041$ (red dash-dotted line in Figs. 2 and 3) the first ECM becomes unstable in a supercritical Hopf bifurcation. The time series displays self-sustained intensity pulsations [see Fig. 4(b)] with the frequency of the ROs, as it is expected for higher pump-currents [Lythe *et al.*, 1997]. The bifurcation diagram for $k > k^H$ shows two branches that scale like the square root of the distance from the bifurcation point (Fig. 3, upper

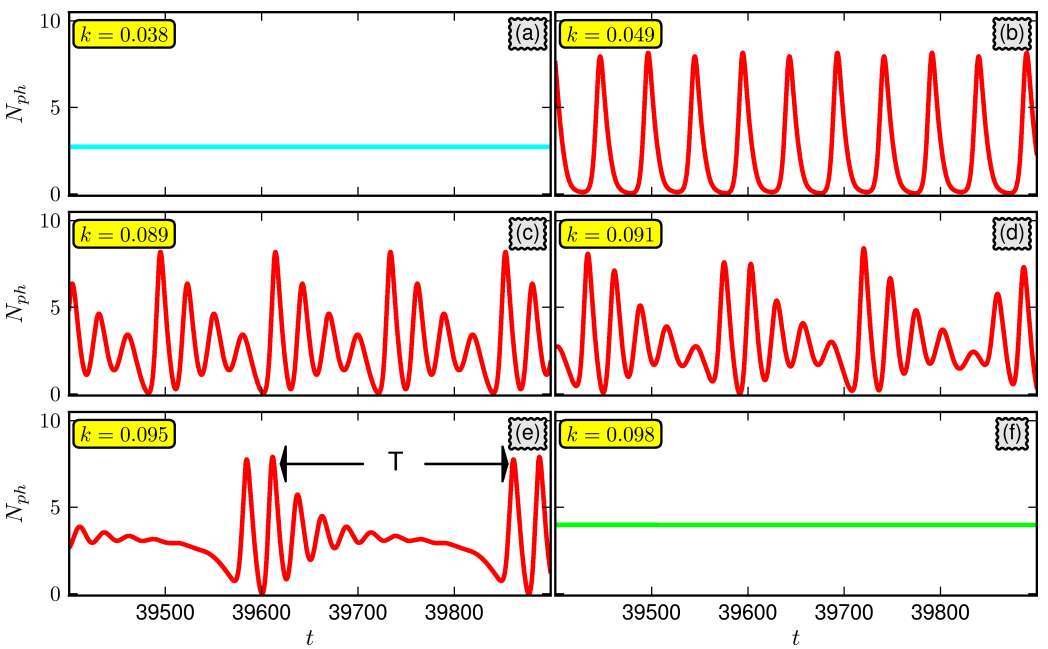

Fig. 4. Time series for selected values of the rescaled feedback strength k. Feedback strengths in (a) to (f) correspond to black dashed lines labeled (a) to (f) in Fig. 3. In (e) the time between two consecutive pulse packages is labeled by T. Parameters: $\alpha = 0.9$, $\tau = 16$, $C = \pi$, other parameters as in Table 1.

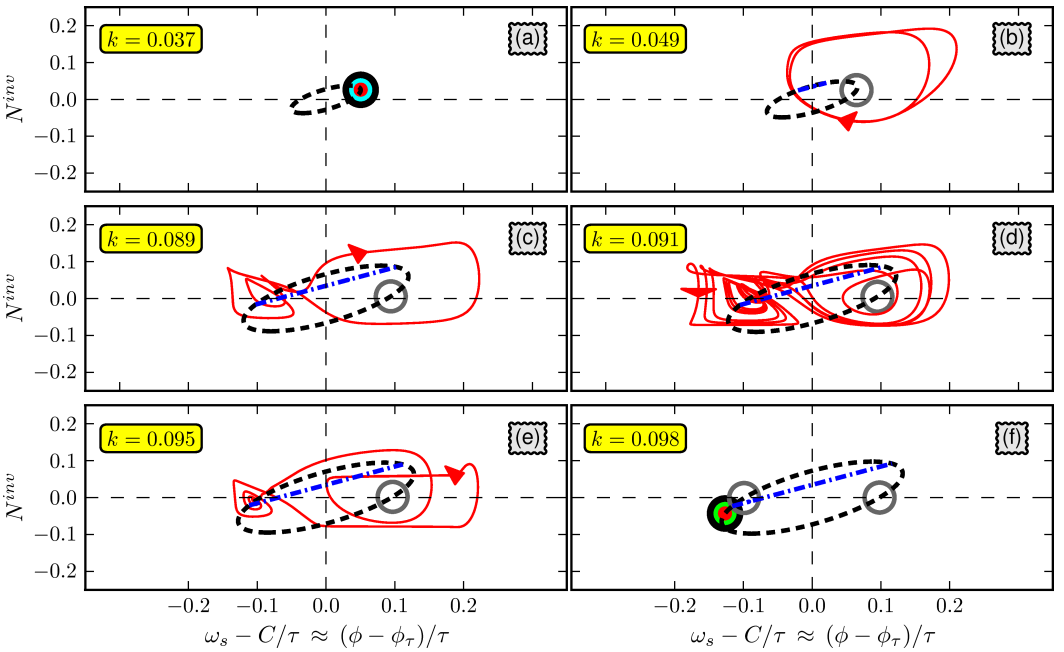

Fig. 5. Phase space projections of the trajectory (red solid line) onto planes spanned by the frequency deviation $\omega_s - C/\tau$ and the inversion N^{inv} for selected values of the rescaled feedback strength k. The stable and unstable ECMs are indicated by filled circles and open gray circles, respectively. The color-code of the stable ECMs is the same as in Fig. 3. The ECMs lie on the ellipse given by Eq. (30) (black dashed line). The blue dash-dotted line is the saddle-node line [Eq. (29)]. Figures (a) to (f) correspond to black dashed lines labeled (a) to (f) in Fig. 3. Parameters: $k = 0.9$, $\tau = 16$, $C = \pi$, other parameters as in Table 1.

panel). This is the signature of a Hopf bifurcation [Kuznetsov, 1995]. In phase space the intensity pulsations correspond to a periodic motion on a delay-induced limit cycle. The Hopf bifurcation is followed by a cascade of period-doubling bifurcations leading to chaos. In Fig. 4(b) (black dashed line (b) in Fig. 3) we see the time series after the first bifurcation of this cascade has taken place. The time series now consists of two oscillations with slightly different peak heights. The corresponding phase space projection in Fig. 5(b) depicts a motion on a two-loop limit cycle. For increasing k the system becomes chaotic. The small chaotic region is followed by a large periodic window ranging from $k = 0.051$ to $k = 0.082$. For larger k-values the laser becomes chaotic again. The chaotic region is interrupted by small windows of frequency locking. Time series and phase space projection of such a frequency locked solution are depicted in Figs. 4(c) and 5(c), respectively (black dashed line (c) in Fig. 3). The time series depicts regular intensity pulsations with the RO frequency. In the phase space projection we note that the attractor has become larger: indeed the trajectory does not only surround the unstable first ECM as it did at the beginning of the bifurcation cascade [Fig. 5(b)], instead it already starts to wind around the point in the phase space, where a new pair of ECMs appears at higher values of k. The winding in the phase space corresponds to the damped ROs in the time series. In Figs. 4(d) and 5(d) we see a time series and a phase space projection in the chaotic region near the end of the bifurcation cascade (dashed line (f) in Fig. 3). The time series displays irregular pulse packages. The underlying frequency is again one of the ROs. In the phase space projection, we recognize the winding mechanism from Fig. 5(c).

At $k = 0.0895$ the time series in Fig. 4(e) shows strictly regular pulse packages (black dashed line (e) in Fig. 3). Note that the long "tail" of the pulse packages in the time series [Fig. 4(e)] corresponds to the winding around the point where the saddle-node bifurcation appears. At the ends of the pulse packages the trajectory is reinjected into the high gain region ($N^{\text{inv}} > 0.1$). A similar reinjection mechanism has previously been observed experimentally and studied theoretically for QW lasers in the short cavity regime [Heil *et al.*, 2001, 2003]. Note that the pulse packages studied by Heil *et al.* [2001, 2003] differ in two ways from the pulse packages described

in this paper: first, their modulation frequency is the external cavity round-trip time which can be attributed to the much lower pump current in their studies as discussed in [Lythe *et al.*, 1997]. Second, the pulse packages studied by Heil *et al.* [2001, 2003] are slightly irregular and thus their trajectory does not close up in the phase space to form a limit cycle. We presume that the second difference could be due to the higher α-factor of $\alpha = 5.0$ the authors use in their numerical studies. We only find strictly regular pulse packages for $\alpha < 1$ and in the short cavity regime. At $k = 0.08955$ a pair of ECMs is created in a saddle-node bifurcation. We can see from Fig. 3 (middle and lower panel) that the second ECM mode is stable upon creation, but with the chosen initial conditions, its basin of attraction is only accessible for the system after a global bifurcation at $k_{\text{bif}} = 0.096$ that we are going to discuss in the following. In [Otto *et al.*, 2010] we found that the time between two consecutive pulse packages T [see Fig. 4(e)] scales logarithmically with the distance from the bifurcation point $k_{\text{bif}} = 0.096$. This behavior is typical for a homoclinic bifurcation of limit cycles with a negative saddle quantity [Kuznetsov, 1995; Hizanidis & Schöll, 2008]. The saddle quantity for a saddle-focus is defined as $\sigma_0 := \lambda_s + \Re(\lambda_{u,\pm})$, where λ_s is the positive real eigenvalue and $\Re(\lambda_{u,\pm})$ are the real parts of the complex conjugate leading eigenvalues, respectively. A negative σ_0 results in the birth of a unique stable limit cycle from a homoclinic orbit. Indeed we find σ_0 to be negative near k_{bif} and the unique limit cycle is the one that is plotted in Fig. 5(e) for $k = 0.095$. For k slightly smaller than k_{bif} we find a small range of bistability between the unique limit cycle and the second ECM mode. For k larger than k_{bif} the laser performs stable continuous wave emission as we can see from the time series [Fig. 4(f)] for $k = 0.098$. The phase space projection [Fig. 5(f)] reveals that now the second ECM is stable (see also black dashed line (g) in Fig. 3).

5. Feedback Tolerance of QD Lasers

In this section we are going to discuss the tolerance of QD lasers to optical feedback. QD lasers are less easily destabilized by optical feedback than QW devices [O'Brien *et al.*, 2003; Huyet *et al.*, 2004; Carroll *et al.*, 2006]. High sensitivity to back-reflected light is one of the major shortcomings of QW laser. According to Huyet *et al.* [2004] the higher tolerance of QD lasers to optical feedback brings the possibility of designing directly modulated semiconductor lasers operating without costly optical isolators that are needed for QW lasers. In this section, we present an analytical formula for the feedback strength k^H at which the QD laser is destabilized in a Hopf bifurcation and compare it to the Hopf bifurcation line we obtained by numerical continuation techniques. From the numerical continuation we find that in the studied parameter range the Hopf bifurcation is super-critical. With the help of the analytics we can attribute the higher feedback tolerance observed for QD laser to their strongly suppressed ROs and their moderate phase-amplitude coupling. For the derivation of the analytical formula for k^H an extensive asymptotic analysis based on the smallness of $\gamma = W/(2\kappa)$, i.e. the ratio of the carrier lifetimes and the photon lifetime, has been performed. Its mathematical details are presented elsewhere [Lüdge, 2011]. For the subsequent discussion it is sufficient to state the expression for k^H:

$$k^H := \frac{-2\Gamma^{\text{Da}}}{\sqrt{1+\alpha^2}(1-\cos(\omega^{\text{Da}}\tau))\cos(\omega_s\tau - \arctan(\alpha))}. \tag{32}$$

In the above equation Γ^{Da} is the damping of the ROs of the solitary laser as introduced in [Lüdge *et al.*, 2011], and it is given by:

$$\Gamma^{\text{Da}} := \frac{1}{2}[N_{\text{ph}}(t_h + \gamma) + \gamma(N_h + t_e^{-1})]. \tag{33}$$

The damping of the ROs Γ^{Da} depends directly on the band-structure of the device through the microscopically calculated scattering rates. The carrier and photon populations are taken at their steady state values without feedback.

In contrast to the damping Γ^{Da} the frequency of the ROs ω^{Da} which is given by

$$\omega^{\text{Da}} := \sqrt{\gamma N_{\text{ph}}} \tag{34}$$

does not explicitly depend on the band-structure. From Eq. (23) we see that within the validity of the approximation of Eq. (24) ω^{Da} shows the square-root-like dependence on the pumping current J that is well known for semiconductor lasers [Erneux & Glorieux, 2010]. From Eq. (32) one can see that the tolerance to optical feedback increases with the damping of the ROs Γ^{Da}, which in turn increases with N_{ph}. From Eq. (23) one sees that N_{ph} and thus the feedback tolerance of the laser increases with the linear gain coefficient g. This is in correspondence with recent experimental findings, where

the impact of the differential gain for the feedback tolerance of the laser is emphasized [Azouigui *et al.*, 2009].

In this paper we discuss the case of very fast holes, where the hole lifetime is drastically smaller than the electron lifetime $t_h \ll t_e$. This case, denoted by the superscript Da in [Lüdge *et al.*, 2011], is appropriate to describe the dynamics of a QD laser with its strongly suppressed ROs [Lüdge & Schöll, 2009; Lüdge *et al.*, 2010]. Note that for the case of similar electron and hole lifetimes that is discussed as "case S" by Lüdge *et al.* [2011] the same expression for k^H is obtained, if we take into account the appropriate damping and frequency of the ROs [Lüdge, 2011].

The expression for k^H [Eq. (32)] has been derived in the limit that the feedback rate k is a small $\mathcal{O}(\gamma)$-quantity and that the external cavity is long, more precisely the following scaling of the parameters has been assumed:

$$k = \mathcal{O}(\gamma), \quad \omega^{\mathrm{Da}} = \mathcal{O}(\gamma^{1/2}), \quad \tau = \mathcal{O}(\gamma^{-1/2}). \tag{35}$$

A similar formula has been previously derived and studied for the LK model [Ritter & Haug, 1993; Levine *et al.*, 1995]. It differs only by the expression for the damping of the ROs. Further, Erneux [2000] refined existing approximations and found appropriate scalings of the parameters leading to different approximations of the Hopf bifurcation point that are better suited for the short cavity regime, large feedback rates as well as operation close to lasing threshold.

For most technological application the phase C of the back-reflected light is not of interest. For example, if one tries to couple the signal of a directly modulated laser into an optical fiber, one does not want to make any effort to control the phase of the back-reflected light. In this case, only the "worst case scenario" might be of interest, namely the minimal feedback strength which can destabilize the laser. From Eq. (32), the following inequalities can be derived:

$$k^H \geq \frac{-\Gamma^{\mathrm{Da}}}{\sqrt{1+\alpha^2}\cos(\omega_s\tau - \arctan(\alpha))} \geq k_c. \tag{36}$$

Here $k_c = \Gamma^{\mathrm{Da}}/(1+\alpha^2)^{1/2}$ is the critical feedback strength as introduced in Eq. (1) with the damping rate $\Gamma_R = \Gamma^{\mathrm{Da}}$ of the ROs. In this paper, we want to study the "worst case" $k^H = k_c$. Therefore we first assume $\cos(\omega^{\mathrm{Da}}\tau) = -1$ to make the first inequality in Eq. (36) hold exactly. Secondly from Eq. (26) we see that in the asymptotic limit, in which Eq. (32) has been derived $\omega_s\tau - C$ is a small $\mathcal{O}(\gamma^{1/2})$-quantity and we thus can assume $\omega_s\tau \approx C$. Within the validity of this approximation the phase

$$C_{\min} := \arctan(\alpha) + (2n+1)\pi, \quad \text{with } n \in \mathbb{Z}, \tag{37}$$

minimizes the expression for k^H [Eq. (32)] with respect to $\omega_s\tau$. For this phase $C_{\min}$ we compare the analytical expression for the Hopf line with the line of the first Hopf bifurcation obtained by numerical continuation in terms of the linewidth enhancement factor α. The numerical continuation has been performed with the program DDE-Biftool [Engelborghs *et al.*, 2002]. In Fig. 6 the curves obtained by numerical continuation are plotted as solid black lines and the analytical approximations are depicted by red dashed lines for the long cavity regime [Fig. 6(a)] and the short cavity regime [Fig. 6(b)], respectively. For a long cavity with $\tau = 80$ we find

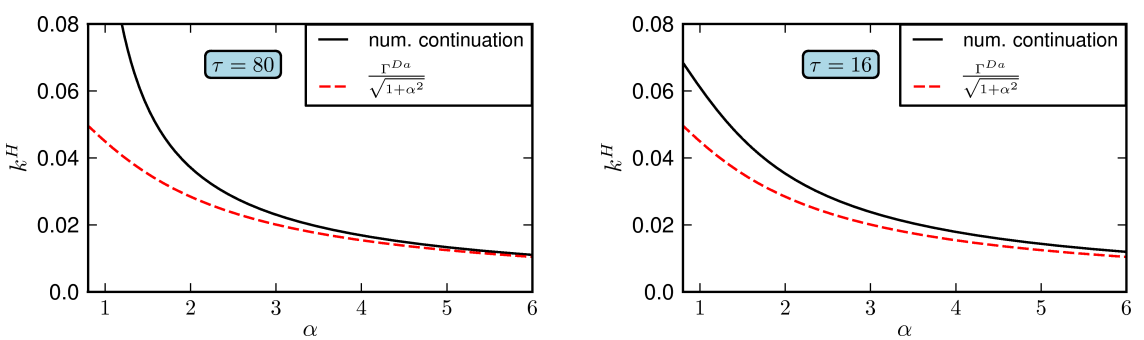

Fig. 6. First Hopf bifurcation for the feedback phase $C_{\min} := \arctan(\alpha) + (2n+1)\pi$ ($n \in \mathbb{Z}$) as a function of the linewidth enhancement factor α. In the long cavity regime for (a) $\tau = 80$ and in the short cavity regime for (b) $\tau = 16$. The black solid lines are obtained by numerical continuation and the red dashed lines are analytical approximations.

very good correspondence for $\alpha \gtrsim 3$. For smaller values of the α-factor the feedback strength k^H becomes so large that the assumption $k^H = \mathcal{O}(\gamma)$ for which Eq. (32) is valid does not hold any longer. That is the reason why the analytic approximation underestimates k^H for small values of α. The same reasoning holds for the short cavity regime $\tau = 16$ [Fig. 6(b)], but the deviations of the analytical and the numerical value for k^H are less pronounced for $\alpha \lesssim 3$, because the feedback strength remains smaller. However, in both cases and for all α-factors in the range studied ($\alpha \in [0.8, 6]$) the analytical formula provides a reliable approximation for the lower bound of k^H.

In the following we are going to discuss the possibility to tune the critical feedback strength k^H by doping of the carrier reservoir. In [Lüdge *et al.*, 2010] the authors discussed that the electron lifetime t_e decreases with increasing n-doping concentration of the carrier reservoir. From Eq. (33) we see that the slower species, namely the electrons ($t_e \gg t_h$), determine the damping of the ROs. This means that the n-doping concentration of the carrier reservoir is an experimentally accessible parameter to control the damping of the ROs, Γ^{Da}, and thus to tune the critical feedback strength, k^H, [Eq. (32)] at which the first feedback induced instability occurs.

6. Conclusion

In this paper, we first discussed the complex dynamics of a semiconductor QD laser subject to optical feedback in the short cavity regime and for a small phase-amplitude coupling expressed by a small value of the α-factor. In this case, we performed a linear stability analysis for the basic solutions and discussed the more complex dynamics in the instability region of the bifurcation diagram. Secondly, an analytical formula for the critical feedback strength k^H at which the QD laser is destabilized in a Hopf bifurcation was presented. With the help of this formula we could explain the higher feedback tolerance of QD lasers found experimentally [Huyet *et al.*, 2004; Carroll *et al.*, 2006] by their strongly suppressed relaxation oscillations and their moderate phase-amplitude coupling which is expressed by moderate α-factors. A comparison of the analytical approximation of k^H with the first Hopf bifurcation line obtained by numerical continuation in terms of the α-factor revealed that the analytics gives a reliable approximation for its lower bound. The approximation holds best for $\alpha \gtrsim 3$, when the critical feedback strength remains small. Finally the possibility to enhance the damping of the ROs and thus the critical feedback strength by n-doping of the carrier reservoir, which is relevant for applications, was discussed.

Acknowledgments

The work of B. Globisch, K. Lüdge and E. Schöll was supported by DFG in the framework of Sfb 787. C. Otto would like to thank the research training group GRK 1558 for support. The work of T. Erneux was supported by the Fond National de la Recherche Scientifique (Belgium) and by the Air Force Office of Scientific Research (AFOSR) grant FA8655-09-1-3068.

References

Azouigui, S., Dagens, B., Lelarge, F., Provost, J. G., Make, D., Le Gouezigou, O., Accard, A., Martinez, A., Merghem, K., Grillot, F., Dehaese, O., Piron, R., Loualiche, S., Zou, Q. & Ramdane, A. [2009] "Optical feedback tolerance of quantum-dot- and quantum-dash-based semiconductor lasers operating at 1.55 μm," *IEEE J. Sel. Topics Quant. Electron.* **15**, 764–773.

Baili, G., Alouini, M., Moronvalle, C., Dolfi, D. & Bretenaker, F. [2006] "Broad-bandwidth shot-noise-limited class-A operation of a monomode semiconductor fiber-based ring laser," *Opt. Lett.* **31**, 62–64.

Baili, G., Alouini, M., Malherbe, T., Dolfi, D., Sagnes, I. & Bretenaker, F. [2009] "Direct observation of the class-B to class-A transition in the dynamical behavior of a semiconductor laser," *EPL* **87**, 44005.

Carroll, O., O'Driscoll, I., Hegarty, S. P., Huyet, G., Houlihan, J., Viktorov, E. A. & Mandel, P. [2006] "Feedback induced instabilities in a quantum dot semiconductor laser," *Opt. Express.* **14**, 10831–10837.

Cong, D. Y., Martinez, A., Merghem, K., Moreau, G., Lemaitre, A., Provost, J. G., Le Gouezigou, O., Fischer, M., Krestnikov, I., Kovsh, A. R. & Ramdane, A. [2007] "Optimisation of α-factor for quantum dot InAs/GaAs Fabry–Perot lasers emitting at 1.3 μm," *Electron. Lett.* **43**, 222–224.

Engelborghs, K., Luzyanina, T. & Roose, D. [2002] "Numerical bifurcation analysis of delay differential equations using DDE-Biftool," *ACM Trans. Math. Softw.* **28**, 1–21.

Erneux, T. [2000] "Asymptotic methods applied to semiconductor laser models," *Proc. SPIE* **3944**, 588–601.

Erneux, T. & Glorieux, P. [2010] *Laser Dynamics* (Cambridge University Press, UK).

Gioannini, M., Sevega, A. & Montrosset, I. [2006] "Simulations of differential gain and linewidth enhancement factor of quantum dot semiconductor lasers," *Opt. Quant. Electron.* **38**, 381–394.

Gioannini, M., The, G. A. P. & Montrosset, I. [2008] "Multi-population rate equation simulation of quantum dot semiconductor lasers with feedback," *Numerical Simulation of Optoelectronic Devices, 2008. NUSOD '08. Int. Conf.*, p. 101.

Globisch, B., Otto, C. Lüdge, K. & Schöll, E. [2012] "Influence of carrier lifetimes on the dynamical behavior of quantum-dot lasers subject to optical feedback," *Phys. Rev. E.*, accepted.

Grillot, F., Naderi, N. A., Pochet, M., Lin, C. Y. & Lester, L. F. [2008] "Variation of the feedback sensitivity in a 1.55 μm InAs/InP quantum-dash Fabry–Perot semiconductor laser," *Appl. Phys. Lett.* **93**, 191108.

Grillot, F. & Dubey, N. [2011] "Influence of the linewidth enhancement factor on the modulation response of a nanostructure-based semiconductor laser operating under external optical feedback," *Proc. SPIE* **7933**, 79330E.

Heil, T., Fischer, I., Elsäßer, W. & Gavrielides, A. [2001] "Dynamics of semiconductor lasers subject to delayed optical feedback: The short cavity regime," *Phys. Rev. Lett.* **87**, 243901.

Heil, T., Fischer, I., Elsäßer, W., Krauskopf, B., Green, K. & Gavrielides, A. [2003] "Delay dynamics of semiconductor lasers with short external cavities: Bifurcation scenarios and mechanisms," *Phys. Rev. E* **67**, 066214.

Hizanidis, J. & Schöll, E. [2008] "Control of noise-induced spatiotemporal patterns in superlattices," *Phys. Stat. Sol.* (*c*) **5**, 207–210.

Huyet, G., O'Brien, D., Hegarty, S. P., McInerney, J. G., Uskov, A. V., Bimberg, D., Ribbat, C., Ustinov, V. M., Zhukov, A. E., Mikhrin, S. S., Kovsh, A. R., White, J. K., Hinzer, K. & Spring Thorpe, A. J. [2004] "Quantum dot semiconductor lasers with optical feedback," *Phys. Stat. Sol.* (*b*) **201**, 345–352.

Krauskopf, B., van Tartwijk, G. H. M. & Gray, G. R. [2000] "Symmetry properties of lasers subject to optical feedback," *Opt. Commun.* **177**, 347–353.

Kuznetsov, Y. A. [1995] *Elements of Applied Bifurcation Theory* (Springer, NY).

Lang, R. & Kobayashi, K. [1980] "External optical feedback effects on semiconductor injection laser properties," *IEEE J. Quant. Electron.* **16**, 347–355.

Levine, A. M., van Tartwijk, G. H. M., Lenstra, D. & Erneux, T. [1995] "Diode lasers with optical feedback: Stability of the maximum gain mode," *Phys. Rev. A* **52**, R3436.

Lin, H. H., Lin, C. H. & Lin, F. Y. [2011] "Four-wave mixing analysis of quantum dot and quantum well lasers," *Opt. Express* **22**, 101–110.

Lingnau, B., Lüdge, K., Chow, W. W. & Schöll, E. [2012] "Many-body effects and self-contained phase dynamics in an optically injected quantum-dot laser," *Semiconductor Lasers and Laser Dynamics V*, eds. Panajotov, K., Sciamanna, M., Valle, A. A. & Michalzik, R. p. 84321J.

Lüdge, K. & Schöll, E. [2009] "Quantum-dot lasers — Desynchronized nonlinear dynamics of electrons and holes," *IEEE J. Quant. Electron.* **45**, 1396–1403.

Lüdge, K., Aust, R., Fiol, G., Stubenrauch, M., Arsenijević, D., Bimberg, D. & Schöll, E. [2010] "Large signal response of semiconductor quantum-dot lasers," *IEEE J. Quant. Electron.* **46**, 1755–1762.

Lüdge, K. & Schöll, E. [2010] "Nonlinear dynamics of doped semiconductor quantum dot lasers," *Eur. Phys. J. D* **58**, 167–174.

Lüdge, K. [2011] *Nonlinear Laser Dynamics — From Quantum Dots to Cryptography* (Wiley-VCH, Weinheim).

Lüdge, K., Schöll, E., Viktorov, E. A. & Erneux, T. [2011] "Analytic approach to modulation properties of quantum dot lasers," *J. Appl. Phys.* **109**, 103112.

Lythe, G., Erneux, T., Gavrielides, A. & Kovanis, V. [1997] "Low pump limit of the bifurcation to periodic intensities in a semiconductor laser subject to external optical feedback," *Phys. Rev. A* **55**, 4443–4448.

Majer, N., Lüdge, K. & Schöll, E. [2010] "Cascading enables ultrafast gain recovery dynamics of quantum dot semiconductor optical amplifiers," *Phys. Rev. B* **82**, 235301.

Mørk, J., Tromborg, B. & Mark, J. [1992] "Chaos in semiconductor lasers with optical feedback — Theory and experiment," *IEEE J. Quant. Electron.* **28**, 93–108.

Newell, T. C., Bossert, D. J., Stintz, A., Fuchs, B., Malloy, K. J. & Lester, L. F. [1999] "Gain and linewidth enhancement factor in InAs quantum-dot laser diodes," *IEEE Phot. Technol. Lett.* **11**, 1527–1529.

O'Brien, D., Hegarty, S. P., Huyet, G., McInerney, J. G., Kettler, T., Lämmlin, M., Bimberg, D., Ustinov, V., Zhukov, A. E., Mikhrin, S. S. & Kovsh, A. R. [2003] "Feedback sensitivity of 1.3 μm InAs/GaAs quantum dot lasers," *Electron. Lett.* **39**, 1819–1820.

Otto, C., Lüdge, K. & Schöll, E. [2010] "Modeling quantum dot lasers with optical feedback: Sensitivity of bifurcation scenarios," *Phys. Stat. Sol.* (*b*) **247**, 829–845.

Pausch, J., Otto, C., Tylaite, E., Majer, N. Schöll, E. & Lüdge, K. [2012]. "Optically injected quantum dot

lasers — impact of nonlinear carrier liftimes on frequency locking dynamics," *New J. Phys.* **14**, 053018.

Ramdane, A., Martinez, A., Azouigui, S., Cong, D. Y., Merghem, K., Akrout, A., Gosset, C., Moreau, G., Lelarge, F., Dagens, B., Provost, J. G., Accard, A., Krestnikov, I. L., Kovsh, A. R. & Fischer, M. E. [2008] "Recent advances in long wavelength quantum dot based lasers," *Proc. SPIE* **6900**, 690008.

Ritter, A. & Haug, H. [1993] "Theory of laser diodes with weak optical feedback. I. Small-signal analysis and side-mode spectra," *J. Opt. Soc. Am. B* **10**, 130–144.

Rottschäfer, V. & Krauskopf, B. [2007] "The ECM-backbone of the Lang–Kobayashi equations: A geometric picture," *Int. J. Bifurcation and Chaos* **17**, 1575–1588.

Schunk, N. & Petermann, K. [1989] "Stability analysis for laser diodes with short external cavities," *IEEE Phot. Technol. Lett.* **1**, 49–51.

van Tartwijk, G. H. M. & Lenstra, D. [1995] "Semiconductor laser with optical injection and feedback," *Quant. Semiclass. Opt.* **7**, 87–143.

van Tartwijk, G. H. M. & Agrawal, G. P. [1998] "Laser instabilities: A modern perspective," *Prog. Quant. Electron.* **22**, 43.

Wegert, M., Majer, N., Lüdge, K., Dommers-Völkel, S., Gomis-Bresco, J., Knorr, A., Woggon, U. & Schöll, E. [2011] "Nonlinear gain dynamics of quantum dot optical amplifiers," *Semicond. Sci. Technol.* **26**, 014008.